Thermal Evolution of the Crystallographic and Magnetic Structure in $LuVO_3$: A Neutron Diffraction Study

A. Muñoz,*,† J. A. Alonso,‡ M. T. Casais,‡ M. J. Martínez-Lope,‡ J. L. Martínez,‡ and M. T. Fernández-Díaz§

Dpto. Física Aplicada, EPS, Universidad Carlos III, Avda. Universidad, 30, E-28911 Leganés-Madrid, Spain, Instituto de Ciencia de Materiales de Madrid, CSIC, Cantoblanco, E-28049 Madrid, Spain, and Institut Laue Langevin, BP 156X, Grenoble, F-38042, France

Received December 11, 2003. Revised Manuscript Received February 16, 2004

Polycrystalline $LuVO_3$ perovskite has been studied by neutron powder diffraction (NPD), specific heat, and magnetization measurements. Below $T_N \approx 107$ K, $LuVO_3$ undergoes magnetic ordering according to a canted antiferromagnetic structure. Neutron diffraction data show that the magnetic structure is characterized by the propagation vector $\mathbf{k} = 0$ and the spin arrangement for the V atoms below T_N is given by the basis vector $(0,A_y,F_z)$. The magnetic structure remains stable down to 2 K and the ferromagnetic component is very weak, in good agreement with the magnetic measurements. The ordered magnetic moment at $T = 2.4$ K for the V atoms is $1.33(6)\mu_B$. A few degrees below T_N, a crystallographic transition is observed, from the orthorhombic room-temperature structure (*Pnma* space group) to monoclinic ($P2_1/n$ space group) below the transition. The changes in the crystallographic structure occur between 94 and 82 K. Despite the fact that below 82 K there are two sites for the V atoms, the arrangement of the V−O bonding lengths is the same in the $y = 0$ plane and in the $y = {}^1/_2$ layer, so the (010) planes are in phase along the *b*-direction. This suggests an in-phase orbital ordering of the V t_{2g} orbitals compatible with the A-type magnetic structure.

Introduction

The transition metal oxides RVO_3 (R = rare-earth and Y) present a distorted orthorhombic perovskite structure of $GdFeO_3$ type at room temperature.[1−4] In the *Pnma* space group description (the long axis parallel to the *b*-direction), the orthorhombic lattice parameters are related to the ideal lattice parameter of the cubic perovskite, a_p, as $a \approx c \approx \sqrt{2}a_p$ and $b \approx 2a_p$.

The first studies carried out on these compounds concerning their magnetic behavior and spin arrangement revealed that the V^{3+} ions order according to a canted antiferromagnetic structure with a T_N ranging from 137 K for $LaVO_3$ to 101 K for $LuVO_3$.[5−9] Below the ordering temperature, the spin arrangement is of G-type for the lighter rare-earths (La−Nd) and A-type for the heavier ones (Ho−Lu and Y) (*Pnma* setting). The coupling of the magnetic moments in the (010) planes is antiferromagnetic both for the G-type and for the A-type; however, the coupling between the (010) layers along the *b* crystallographic direction is ferromagnetic for the G-type and antiferromagnetic for the A-type.

The discovery of a peculiar phenomenon, known as anomalous diamagnetism, in $LaVO_3$,[10−12] enormously renewed the interest in these compounds, in particular in the perovskites with lighter rare earths. These works revealed that this novel phenomenon is also present in another members of the family, as $CeVO_3$ and YVO_3.[13−15] The anomalous diamagnetism consists of a reversal of the weak ferromagnetic component below a characteristic temperature T_t, some degrees below T_N. It has been suggested that the reversal of the weak ferromagnetic component is caused by a first-order magnetostrictive transition that occurs at T_t due to a cooperative Jahn−Teller distortion.[15−16] The magnetostrictive distortion

* Corresponding author. E-mail: amunoz@fis.uc3m.es.
† Universidad Carlos III.
‡ Instituto de Ciencia de Materiales de Madrid, CSIC.
§ Institut Laue Langevin.

(1) Yakel, H. L. *Acta Crystallogr.* **1955**, *8*, 394.
(2) Bertaut, F.; Forrat, F. *J. Phys. Radium* **1956**, *17*, 129.
(3) Geller, S. *Acta Crystallogr.* **1957**, *10*, 243.
(4) Bordet, P.; Chaillout, C.; Marezio, M.; Huang, Q.; Santoro, A.; Cheong, S−W.; Takag, H.; Oglesby, C. S.; Batlogg, B. *J. Solid State Chem.* **1993**, *106*, 253.
(5) Borukhovich, A. S.; Bazuev, G. V.; Shveikin, G. P. *Sov. Phys. Solid State* **1973**, *15*, 2203.
(6) Borukhovich, A. S.; Bazuev, G. V.; Shveikin, G. P. *Sov. Phys. Solid State* **1974**, *16*, 286.
(7) Borukhovich, A. S.; Bazuev, G. V. *Sov. Phys. Solid State* **1974**, *16*, 273.
(8) Zubkov, V. G.; Bazuev, G. V.; Shveikin, G. P. *Sov. Phys. Solid State* **1976**, *18*, 1165.
(9) Borukhovich, A. S.; Zubkov, V. G.; Bazuev, G. V. *Sov. Phys. Solid State* **1978**, *20*, 1049.
(10) Shirakawa, N.; Ishikawa, M. *Jpn. J. Appl. Phys.* **1991**, *30*, L 755.
(11) Mahajan, A. V.; Johnston, D. C.; Torgeson, D. R.; Borsa, F. *Physica C* **1991**, *185−189*, 1095.
(12) Mahajan, A. V.; Johnston, D. C.; Torgeson, D. R.; Borsa, F. *Phys. Rev. B* **1992**, *46*, 10966.
(13) Nguyen, H. C.; Goodenough, J. B. *Phys. Rev. B* **1995**, *52*, 324.
(14) Nguyen, H. C.; Goodenough, J. B. *J. Solid State Chem.* **1995**, *119*, 24.
(15) Ren, Y.; Palstra, T. T. M.; Khomskii, D. I.; Nugroho, A. A.; Menovsky, A. A.; Sawatzky, G. A. *Nature* **1998**, *396*, 441.
(16) Goodenough, J. B.; Nguyen, H. C. *C. R. Acad. Sci., Ser. IIb: Mec., Phys., Chim., Astron.* **1994**, *319*, 1285.

10.1021/cm035314a CCC: $27.50
Published on Web 03/23/2004

induces a change in the crystallographic structure, which becomes monoclinic below T_t, as it has been shown for $LaVO_3$,[4] $CeVO_3$[17−18], YVO_3[19] and $YbVO_3$.[20]

In the ideal cubic perovskite, the crystal field associated with the VO_6 octahedra splits the V $3d^2$ orbitals, giving a $t_{2g}^2e_g^0$ electronic configuration for the V^{3+} ions, with a 3-fold orbital degeneracy for the t_{2g} level. The orthorhombic distortion splits the t_{2g}^2 orbitals into a doublet and a singlet. At room temperature, the RVO_3 compounds present an O-type distortion with $b/(c\sqrt{2}) > 1$, which implies that the ground state is the doublet; however, below T_t, and for the lighter members of the series, the distortion becomes O′-type with $b/(c\sqrt{2}) < 1$, and the ground state is the singlet. A lot of attention has been paid to the interplay between the t_{2g} orbital ordering and the lattice distortion, in particular, in $LaVO_3$, $CeVO_3$, and YVO_3.[17,19,21−22] From a crystallographic point of view, the Jahn−Teller distortion of the VO_6 octahedra and the changes in the orbital ordering are inferred from the local arrangement of the V−O distances in the (010) planes. At room temperature, the short and the long V−O distances alternate along the [101] and [10$\bar{1}$] directions in the (010) planes, and these planes present the same arrangement along the *b*-direction (they are "in phase"). This orbital ordering is compatible with the A-type magnetic ordering (*Pnma* setting). Below T_t, two different sites for the V atoms appear, and the arrangement of the V−O distances in the (010) layers can vary along the *b*-direction ("out of phase"), which is compatible with a G-type magnetic ordering. In all the compounds of the family for which this point has been analyzed, there is a coherence between the magnetic ordering and the type of orbital ordering. This seems to indicate that the type of orbital ordering determines the antiferromagnetic structure. YVO_3 represents the transition between both situations. Below $T_N = 118$ K, a G-type magnetic structure is found, compatible with the out-of-phase arrangement of the V−O bonding distances found in the successive (010) planes along the *b*-direction. Below $T_s \approx 77$ K a transition to an in-phase orbital ordering takes place in good agreement with the A-type magnetic structure found below this temperature[23] (*Pnma* setting).

To complete this picture, in this paper we present a detailed study on the last member of the series, $LuVO_3$. The evolution of both the crystallographic and the magnetic structure is analyzed from neutron powder diffraction (NPD) data. The NPD measurements are complemented by susceptibility and specific heat macroscopic measurements.

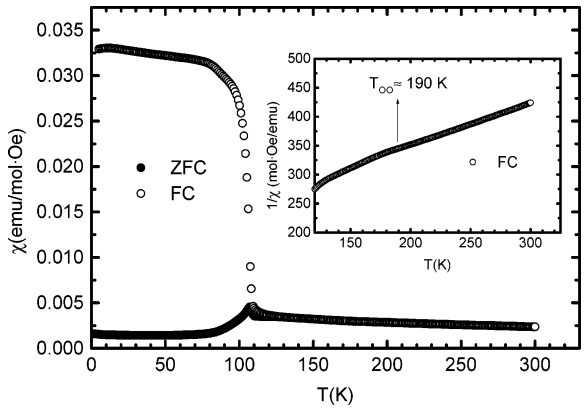

Figure 1. Thermal evolution of the susceptibility measured under a 0.5 kOe magnetic field, in zero field-cooling (ZFC) and field-cooling (FC) conditions. Inset: Thermal evolution of the inverse of the susceptibility (FC) for $120 < T < 300$ K.

Experimental Section

$LuVO_3$ perovskite was prepared in polycrystalline form by reduction of the $LuVO_4$ precursor, previously obtained by solid sate reactions. Stoichiometric amounts of analytical grade Lu_2O_3 and NH_4VO_3 were ground and heated at 1173 K for 12 h, then reground and fired at 1273 K for 12 h in air; the X-ray diffraction diagram of the resulting powder corresponded to pure $LuVO_4$. The final reduction process of this material was performed at 1433 K for 12 h in a H_2/N_2 (15%/85%) flow.

The DC susceptibility measurements were performed in a commercial SQUID magnetometer. The zero-field cooling (ZFC) susceptibility curve was obtained in the temperature interval $1.9 < T < 200$ K, and the field-cooling (FC) curve was obtained for $5 < T < 300$ K; in both cases, a 0.5 kOe magnetic field was applied. The specific heat measurements were carried out in a semiadabatic He calorimeter with a ^{3}He insert, using the heat-pulsed method for temperatures going from 0.5 to 275 K under a zero magnetic field. It was measured in a pellet sintered at 1433 K in a H_2/N_2 flow. To determine the lattice contribution to the specific heat, the heat capacity for the isostructural and nonmagnetic $LaScO_3$ perovskite was also measured for $1.8 < T < 164.8$ K.

High-resolution NPD patterns were acquired at room temperature and at $T = 2$ K at the D2B diffractometer of the Institut Laue-Langevin in Grenoble (France), with a wavelength of 1.594 Å. A set of NPD patterns was also dynamically collected in the temperature range $2.3 < T < 183.7$ K with a wavelength $\lambda = 2.524$ Å in the D1B diffractometer, and for $2.9 < T < 295.8$ K with $\lambda = 1.305$ Å at the high-flux D20 diffractometer. The NPD data with $\lambda = 2.524$ Å were used to study the magnetic structure and its thermal evolution. The NPD data collected with $\lambda = 1.305$ Å were used to analyze the changes in the crystallographic structure. The neutron diffraction data were analyzed by the Rietveld method,[24] using the FULLPROF program.[25] In the refinement, the profile was simulated by a pseudo-Voigt function and the background was fitted with a fifth-degree polynomial function.

Results

Magnetic Measurements. The zero field-cooling (ZFC) and the field-cooling (FC) susceptibility curves are presented in Figure 1. On decreasing temperature, the ZFC curve exhibits an anomaly below 110 K, and after showing a maximum at around $T_N \approx 107$ K, the susceptibility decreases, indicating the appearance of a magnetic order. The FC susceptibility separates from the ZFC curve behavior below T_N, in good agreement

(17) Ren, Y.; Nugroho, A. A.; Menovsky, A. A.; Strempfer, J.; Rütt, U.; Iga, F.; Takabatake, T.; Kimbal, C. W. *Phys. Rev. B* **2003**, *67*, 1014107.
(18) Muñoz, A.; Alonso, J. A.; Casais, M. T.; Martínez-Lope, M. J.; Martínez, J. L.; Fernández-Díaz, M. T. *Phys. Rev. B* **2003**, *68*, 144429.
(19) Blake, G. R.; Palstra, T. T. M.; Ren, Y.; Nugroho, A. A.; Menovsky, A. A. *Phys. Rev. Lett.* **2001**, *87*, 245501.
(20) Muñoz, A.; Alonso, J. A.; Casais, M. T.; Martínez-Lope, M. J.; Martínez, J. L.; Fernández-Díaz, M. T. *J. Mater. Chem.* **2003**, *13*, 1234−40.
(21) Sawada, H.; Hamada, N.; Terakura, K.; Asada, T. *Phys. Rev. B* **1996**, *53*, 12742.
(22) Mizokawa, T.; Khomskii, D. I.; Sawatzky, G. A. *Phys. Rev. B* **1999**, *60*, 7309.
(23) Kawano, H.; Yoshizawa, H.; Ueda, Y. *J. Phys. Soc. Jpn.* **1994**, *63*, 2857−2861.
(24) Rietveld, H. M. *J. Appl. Crystallogr.* **1969**, *2*, 65.
(25) Rodríguez-Carvajal, J. *Physica B* **1993**, *192*, 55.

Table 1. Lattice Parameters for $LuVO_3$

	space group	*a*(Å)	*b*(Å)	*c*(Å)	α(°)	vol(Å^3)
RT	*Pnma*	5.5607(2)	7.5344(2)	5.2153(2)		218.502(11)
$T = 2$ K	$P2_1/n$ 1 1	5.54335(11)	7.51125(15)	5.21723(10)	89.993(4)	217.232(7)

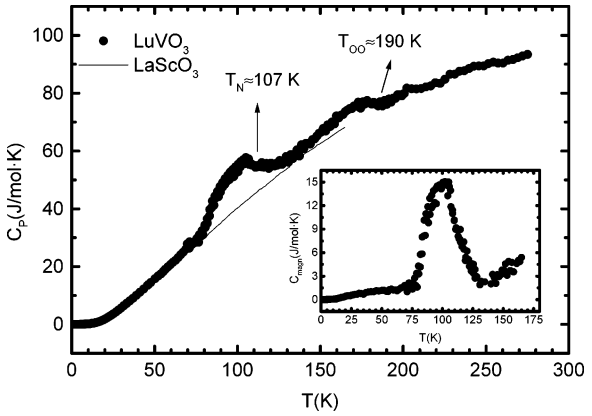

Figure 2. Temperature dependence of the specific heat without magnetic field for $LuVO_3$ and for a reference sample of $LaScO_3$. Inset: Magnetic contribution to the specific heat in $LuVO_3$.

with the onset of a magnetic order. It exhibits an important increase below T_N. Above the ordering temperature, the susceptibility suffers a significant change in the slope at around $T_{OO} \approx 190$ K (inset in Figure 1), and in the temperature range $240 < T < 300$ K the inverse of the susceptibility seems to vary linearly with temperature. In this temperature interval, and in a first approximation, the susceptibility has been fitted according to the Curie−Weiss law. The fit gives a paramagnetic temperature $\Theta_P = -276(1)$ K and an effective magnetic moment $\mu_{eff} = 3.3(1)\,\mu_B$. This value is slightly above the theoretical one for the V^{3+} ions, $\mu_{eff}(V^{3+}) = 2.83\,\mu_B$ (spin only, $S = 1$).

Specific Heat Measurements. In Figure 2, the specific heat is plotted as C_P versus T. On decreasing the temperature, a first anomaly is observed at around $T_{OO} \approx 190$ K, which, as will be discussed later, is linked to the appearance of an orbital ordering in $LuVO_3$. On the other hand, a sharp increase of the heat capacity is observed at around T_N, in good agreement with the susceptibility measurements. However, the anomaly spreads down to 80 K, as will be shown in the NPD data, because a crystallographic transition appears a few degrees below T_N, which does not clearly appear separated from the magnetic transition in the specific heat curve.

The contribution to the specific heat coming from the lattice vibrations has been estimated from the specific heat of the nonmagnetic and isostructural compound $LaScO_3$, measured in the temperature interval $1.8 < T < 164.8$ K (see Figure 2). It is assumed that the lattice contribution to the specific heat in $LuVO_3$ is the same as in $LaScO_3$. Thus, the magnetic contribution to the specific heat in $LuVO_3$ can be estimated by a simple subtraction of both curves. The magnetic contribution calculated in this way is plotted in the inset of Figure 2. In the curve, only an anomaly appears at around T_N. The entropy change that takes place below the ordering temperature can be evaluated from the curve of the magnetic specific heat through the expression $\int(C_{magn}/T)dT$. In the temperature interval $2 < T < 144$ K, the corresponding entropy change is $\Delta S = 6.41$ J/mol K. On taking into consideration that the ground state of the V^{3+} ions is $^3F_2$, and as the magnetic moment is only given by the spin $S = 1$, the calculated entropy change is $\Delta S = R\ln(2S + 1) = R\ln(3) = 9.13$ J/mol·K. Therefore, the experimental entropy change represents about 70% of the theoretical one.

Table 2. Structural Parameters Obtained from the Rietveld Refinement of the NPD Patterns with $\lambda = 1.594$ Å

atom	position	RT (*Pnma*)	$T = 2$ K ($P2_1/n$ 1 1)
Lu	*x*	0.0709(3)	0.0738(2)
	y	0.25	0.2507(5)
	z	0.9791(3)	0.9761(2)
	B(Å^2)	0.42(3)	0.19(2)
V1	*x*	0.50	0.50
	y	0.00	0.00
	z	0.00	0.00
	B(Å^2)	0.4	0.20
V2	*x*		0.00
	y		0.00
	z		0.50
	B(Å^2)		0.20
O1	*x*	0.4546(4)	0.4562(2)
	y	0.25	0.2503(6)
	z	0.1194(4)	0.1217(3)
	B(Å^2)	0.55(4)	0.43(3)
O2	*x*	0.3071(3)	0.2985(9)
	y	0.0603(2)	0.0600(5)
	z	0.6888(3)	0.6811(7)
	B(Å^2)	0.59(2)	0.22(6)
O3	*x*		0.1937(10)
	y		0.9379(5)
	z		0.1881(7)
	B(Å^2)		0.60(7)
discrep. factors	R_p	3.4%	3.3%
	R_{wp}	4.3%	4.2%
	R_{Bragg}	4.0%	3.9%
	χ^2	1.1	1.7

Neutron Diffraction Measurements. *Crystallographic Structure.* A high-resolution NPD pattern acquired with a wavelength $\lambda = 1.594$ Å was used for the refinement of the crystallographic structure at room temperature (RT). All the reflections of the pattern could be indexed by using the orthorhombic space group *Pnma* and with the lattice parameters shown in Table 1. The atomic positions and some selected atomic distances of the RT crystal structure are listed in Tables 2 and 3, respectively. The goodness of the fit is displayed in Figure 3a, showing the experimental and calculated NPD profiles after the Rietveld refinement.

For the analysis of the thermal evolution of the crystallographic structure, a set of sequential NPD patterns collected in the temperature range $2.9 < T < 295.8$ K with $\lambda = 1.305$ Å were taken into consideration. On decreasing the temperature below T_N, between 94 and 82 K, some changes are observed on the Bragg reflections that suggest a crystallographic transition. These changes can be explained by a symmetry lowering from orthorhombic to monoclinic. This is illustrated in

Table 3. Selected Inter-Atomic Distances (in Å)[a]

	RT (*Pnma*)	*T* = 2 K ($P2_1/n$ 1 1)	
Lu−O1	2.255(3)	2.252(2)	
Lu−O1	2.192(3)	2.198(2)	
Lu−O2	(×2) 2.2227(2)	2.241(5)	
Lu−O2	(×2) 2.462(2)	2.444(5)	
Lu−O2	(×2) 2.669(2)	2.654(5)	
Lu−O3		2.223(5)	
Lu−O3		2.428(5)	
Lu−O3		2.680(5)	
<Lu−O>	2.3953(7)	2.390(5)	
V−O1 (×2)	1.9998(6)	V1−O1 (×2)	1.999(4)
V−O2 (×2)	1.9978(14)	V1−O3 (×2)	2.016(5)
V−O2′ (×2)	2.0230(15)	V1−O2 (×2)	2.054(4)
		V2−O1 (×2)	1.995(4)
		V2−O3 (×2)	2.005(4)
		V2−O2 (×2)	1.958(5)
<V−O>	2.0069(5)		2.004(5)

[a] V1 is at ($^1/_2$,0,0) and V2 is at (0,0,$^1/_2$).

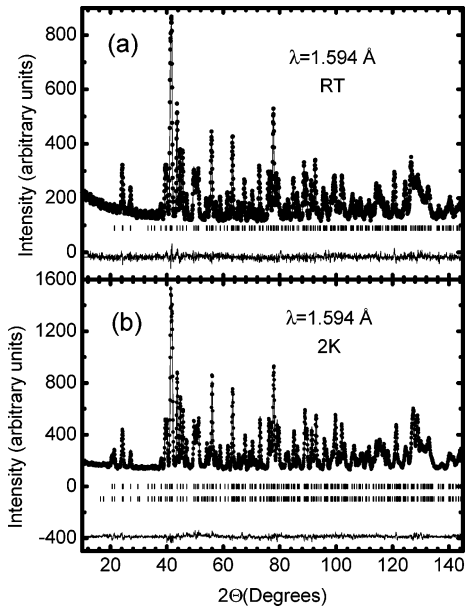

Figure 3. Observed (solid circles), calculated (solid line), and difference (bottom line) NPD patterns: (a) NPD at room temperature and (b) NPD pattern at *T* = 2 K. The first row of tic marks corresponds to the Bragg reflections of $LuVO_3$, and the second row (in (b)) corresponds to the magnetic peaks.

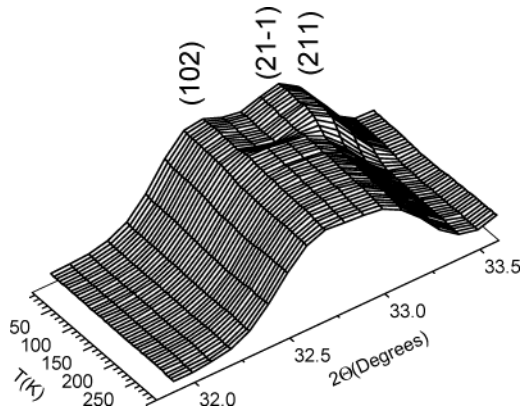

Figure 4. Thermal variation of the nuclear peaks located in the angular range 31.8 < 2Θ < 33.6.

Figure 4, where the thermal variation of the nuclear peaks located in the angular range 31.8 < 2Θ < 33.6 is given. The (211) Bragg reflection (*Pnma*) undergoes an enlargement below 94 K, which is due to the appearance of the (21$\bar{1}$) Bragg reflection upon the transition to monoclinic symmetry.

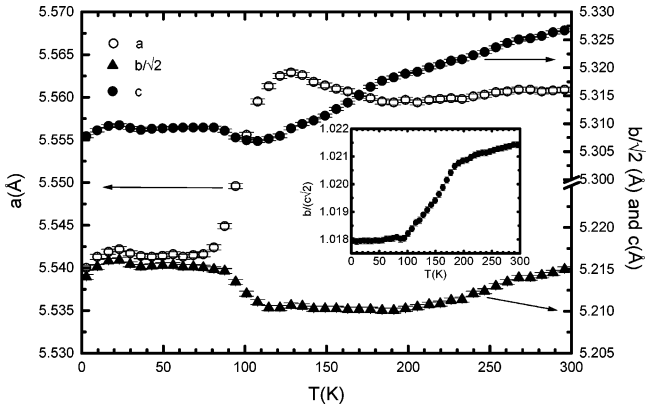

Figure 5. Thermal variation of the lattice parameters. For 94.3 < *T* < 295.8 K, *Pnma* space group; and for 2.4 < *T* < 94.3 K, $P2_1/n$ space group. Inset: Thermal evolution of the ratio $\mathbf{b}/(\sqrt{2}\mathbf{c})$.

The refinement of the monoclinic structure was performed from a NPD pattern collected at 2 K with λ = 1.594 Å. The pattern was fitted with the $P2_1/n$ (C_{2h}^5) monoclinic space group (the 2-fold axis parallel to *a*) and the spin arrangement obtained in the magnetic structure resolution was also taken into consideration. The good agreement between the calculated and experimental patterns is shown in Figure 3b. The lattice parameters and the atomic positions obtained in the fitting are shown in Tables 1 and 2. In the $P2_1/n$ phase there are two crystallographically independent V positions (V1 and V2), as well as 3 types of nonequivalent oxygen atoms (O1, O2, and O3) all in general positions. The α parameter that reflects the low-temperature monoclinic distortion (89.993(4)°) slightly deviates from 90°, what indicates a strongly pseudo-orthorhombic unit cell.

The thermal evolution of the lattice parameters in the temperature range 2.9 < *T* < 295.8 K is shown in Figure 5. Important changes are observed between 80 and 110 K, coinciding with the phase transition below T_N. The *b* and *c* parameters undergo a sudden increase between 80 and 90 K, whereas the *a* parameter experiences an important contraction near the crystallographic transition. On the other hand, on decreasing temperature below 190 K, and coinciding with the anomaly observed in the specific heat curve, there is a noticeable anomaly in the thermal variation of the lattice parameters. Another important feature of the RVO_3 compounds is the type of the orthorhombic distortion that is defined by the ratio $b/(c\sqrt{2})$. According to the inset of Figure 5, $b/(c\sqrt{2}) > 1$ for all the temperature range, as corresponding to a O-type distortion. However, the ratio continuously decreases below 190 K and reaches a plateau below 90 K.

The thermal evolution of the V−O bond lengths, characteristic of the VO_6 octahedra, is plotted in Figure 6. Below 94.3 K the $P2_1/n$ monoclinic space group has been considered, and the V−O distances represented in Figure 6 are an average of the corresponding V1−O and V2−O distances. The most important changes take place in the V−O distances placed in the ac plane. First, at around 190 K the V−O distances in the *ac* plane, which are similar to the V−O distance along *b*, start to separate from one another. This implies a change in the distortion of the VO_6 octahedra, which can indicate a change in the orbital ordering, in good agreement with

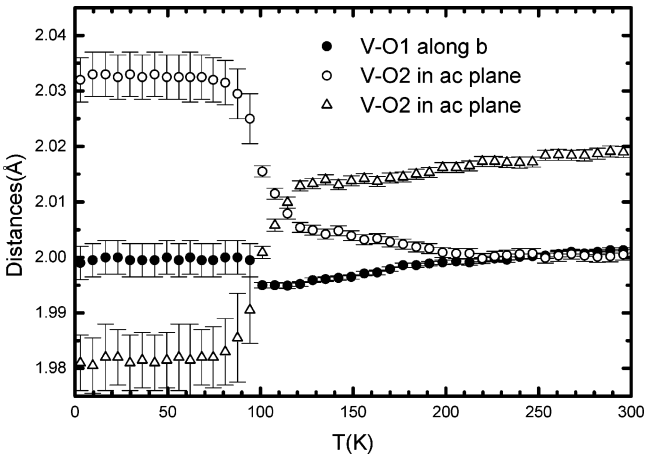

Figure 6. Thermal variation of the V−O atomic distances. Below 94.3 K the V−O distances are the average of the V1−O and V2−O distances.

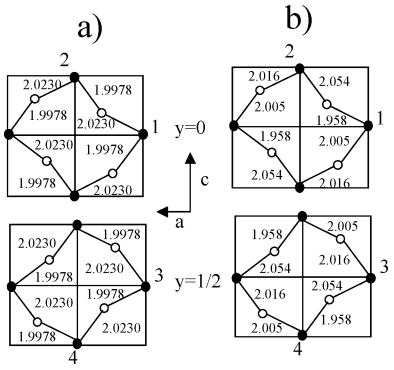

Figure 7. V−O bonding distances: (a) at RT and (b) at T = 2 K

the anomalies observed in the susceptibility and in the specific heat. On the other hand, the V−O distances in the *ac* plane drastically change between 80 and 110 K, with the longest V−O distance becoming the shortest one, and vice-versa.

Finally, concerning the V−O distances in the *ac* plane in the monoclinic phase, it is important to point out that, despite the existence of two sites for the V atoms, the arrangement of the V−O distances in the $y = 0$ plane is "in phase" with the arrangement of the distances in the $y = {}^1/_2$ plane. This can be seen in Figure 7, where the distances calculated at $T = 2$ K are represented.

Magnetic Structure Resolution. The magnetic structure was analyzed from the NPD patterns acquired in the temperature range $2.3 < T < 183.7$ K with $\lambda = 2.524$ Å. On decreasing temperature below 109 K, some Bragg reflections forbidden by the *Pnma* space group start to be observed, as the (110) reflection. Also, the intensity of other weak reflections, as (011), undergo an important increase (Figure 8). This indicates the onset of a magnetic ordering, in good agreement with the susceptibility and specific heat measurements. The magnetic structure is characterized by the propagation vector $k = 0$, and the only magnetic reflections observed are those with $k = 2n + 1$ and $h + l = 2n + 1$. Below T_N, the intensities of the magnetic reflections monotonically increase and they seem to reach saturation at low temperature, therefore the magnetic structure remains stable up to 2 K.

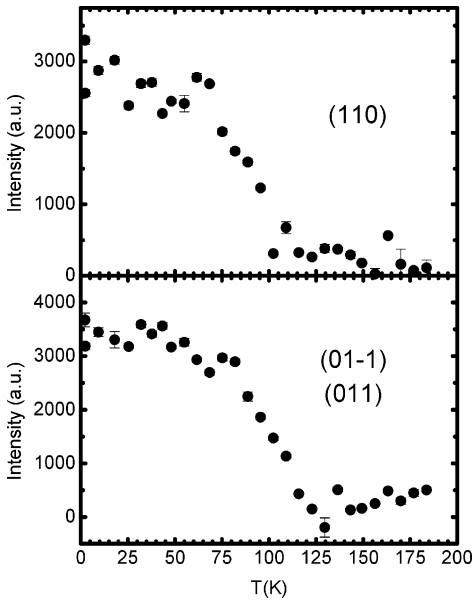

Figure 8. Thermal variation of the magnetic peaks (110) and (01−1)+(011) ($P2_1/n$ space group). The reflections are (110) and (011), respectively, in the *Pnma* space group.

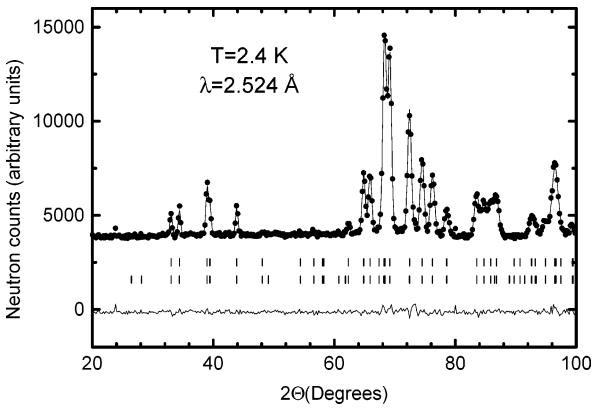

Figure 9. Observed (solid circles), calculated (solid line), and difference (bottom line) NPD patterns for $T = 2.4$ K. The first row of tic marks corresponds to the Bragg reflections of $LuVO_3$ and the second row corresponds to the magnetic peaks.

For the resolution of the magnetic structure, we have considered those solutions compatible with the symmetry of the space group. For $k = 0$ and for the *Pnma* space group the solutions are given in ref 26. For the $P2_1/n$ space group, only those solutions with equal magnetic moment for the two vanadium sites, V1 and V2, have been taken into consideration.[18] Let us point out that, in the magnetic structure resolution, the crystallographic structure has been considered orthorhombic in the temperature range $94.3 < T < 107$ K and monoclinic for $T < 94.3$ K. After checking the different solutions, the one leading to the lowest discrepancy factors between calculated and observed magnetic intensities is $(0,A_y,F_z)$ (*Pnma* setting). For the A_y vector the relationships among the magnetic moments is $m_{1y} = -m_{2y} = -m_{3y} = m_{4y}$ and for the F_z vector $m_{1z} = m_{2z} = m_{3z} = m_{4z}$. The notation for the V atoms is 1 $(0,0,{}^1/_2)$, 2$({}^1/_2,0,0)$, 3$(0,{}^1/_2,{}^1/_2)$, and 4$({}^1/_2,{}^1/_2,0)$. The experimental and calculated patterns after the full refinement of the magnetic structure at $T = 2.4$ K are compared in Figure

(26) Muñoz, A.; Alonso, J. A.; Martínez-Lope, M. J.; García-Muñoz, J. L.; Fernández-Díaz, M. T. *J. Phys. Condens. Matter* **2000**, *12*, 1361.

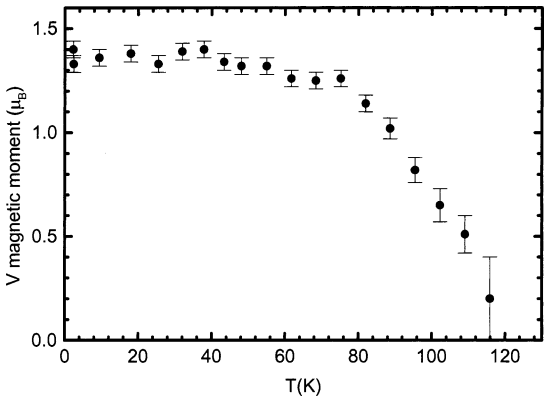

Figure 10. Thermal evolution of the ordered magnetic moments for the V^{3+} ions.

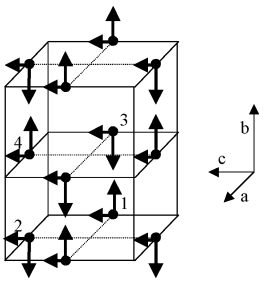

Figure 11. View of the magnetic structure of $LuVO_3$. For the sake of clarity, only V atoms are represented.

Table 4. Results from the Magnetic Structure Determination Corresponding to $T = 2.4$ K

	V^{3+}
solution	$(0,A_y,F_z)$
values(μ_B)	(0,1.32(4),−0.1(3))
$\|\mathbf{m}\|$ (μ_B)	1.33(6)
discrep. factors	R_B(nuclear) = 3.2
	R_B(magnet.) = 2.4
	$\chi^2 = 2.2$

9. As it is displayed in Table 4, the refined magnetic moment at $T = 2.4$ K is 1.33(6) μ_B. Let us point out that the ferromagnetic component is negligible: for instance, the ferromagnetic component is −0.1(3) μ_B at $T = 2.4$ K, which confirms the presence of a weak ferromagnetism in this compound. The thermal evolution of the magnetic moment is presented in Figure 10. A sketch of the magnetic structure is presented in Figure 11: if only the component along the *b*-direction is considered, the solution implies an antiferromagnetic coupling of the magnetic moments in the (010) planes, which are also antiferromagnetically coupled along the *b*-direction.

Discussion

The magnetic measurements have confirmed that $LuVO_3$ presents a magnetic ordering with $T_N \approx 107$ K. The study of the magnetic structure from neutron diffraction data has shown that the spin arrangement for the V atoms below T_N is given by the basis vector $(0,A_y,F_z)$ (*Pnma* setting, ref 27). The magnetic structure remains stable down to 2 K and the ferromagnetic component is very weak, in good agreement with the presence of a weak ferromagnetism effect observed in the magnetic measurements. The magnetic moment at $T = 2.4$ K for the V atoms is 1.33(6)μ_B, therefore the electronic configuration is $3d^2$, as expected for the vanadium ions with a +3 oxidation state.

The study of the evolution of the crystallographic structure has shown that it is orthorhombic at room temperature, *Pnma* space group, but it becomes monoclinic at low temperature, $P2_1/n11$ space group. According to the NPD data, the crystallographic transition takes place below the ordering temperature, and although it is difficult to give a precise value for the transition temperature, the structural rearrangement occurs between 94 and 82 K. Despite that below 82 K there are two sites for the V atoms, the arrangement of the V−O bonding lengths is the same in the $y = 0$ and $y = {}^1/_2$ planes, thus the (010) planes are in phase along the *b*-direction. On the other hand, in all the temperature range the ratio $b/(\sqrt{2}c) > 1$ is kept, which corresponds to a O-type distortion. In this case, the t_{2g}^2 electronic configuration adopted by the d^2 electrons splits into a singlet and a doublet because of the crystal field effects, and the ground state is the doublet.[13]

It is worthwhile comparing the spin arrangement found in the lighter RVO_3 compounds, as in $CeVO_3$, $(F_x,0,G_z)$ (*Pnma* setting), with the spin arrangement of the heavier ones, as in $LuVO_3$, $(0,A_y,F_z)$. As in both cases the ferromagnetic component is weak (F_x and F_z, respectively), both types of magnetic ordering can be named as G-type and A-type, respectively. In both situations, the magnetic moments exhibit an antiferromagnetic arrangement within the (010) plane; in the G-type the (010) planes are ferromagnetically coupled along the *b*-direction, whereas for the A-type the coupling between adjacent planes is antiferromagnetic. This is related to the particular arrangement of the V−O bonds: in the lighter RVO_3 compounds, the arrangement of the V−O bonding lengths in the $y = 0$ and $y = {}^1/_2$ plane is different, which yields to an out-of-phase orbital ordering. In contrast, in the heavier compounds the arrangement of the V−O bonding lengths is similar in both planes, giving rise to an in-phase orbital ordering. Therefore, an in-phase orbital ordering seems to favor an antiferromagnetic coupling of the moments between the (010) planes along *b*, whereas an out-of-phase orbital ordering implies a ferromagnetic coupling of the (010) planes.

It has been predicted that a larger degree of octahedral tilting stabilizes the in-phase orbital ordering,[22] whereas the contrary stabilizes the out-of-phase orbital ordering. This trend is also observed in $LuVO_3$, which shows the largest degree of octahedral tilting of the whole series. The average <V−O−V> angle at RT is 142.2° in $LuVO_3$, slightly more bent than that observed in $YbVO_3$ of 142.5°.[20] As we have seen before, the A-type is concomitant with an in-phase orbital ordering, as observed in $LuVO_3$.

On the other hand, for the lighter compounds, below the crystallographic transition, the distortion is O′-type with $b/(\sqrt{2}c) < 1$, and the ground state corresponding to the levels in which the $t_{2g}^2 e_g^0$ level splits, is the

(27) The equivalence between the basis vectors given in the *Pbnm* (long axis along *c*) and *Pnma* (long axis along *b*) settings is obtained after the following considerations. First, the relationship between the lattice parameters (*a*′,*b*′,*c*′) (*Pbnm*) and (*a*, *b*, *c*) (*Pnma*) is *a*′→*c*; *b*′→*a*; *c*′→*b*. Second, the relationship between the atoms notation (*Pbnm*→*Pnma*) is 1′(${}^1/_2$, 0, 0)→1(0, 0, ${}^1/_2$); 2′(${}^1/_2$, 0, ${}^1/_2$)→3(0, ${}^1/_2$, ${}^1/_2$); 3′(0, ${}^1/_2$, ${}^1/_2$)→4(${}^1/_2$, ${}^1/_2$, 0); 4′(0, ${}^1/_2$, 0)→2(${}^1/_2$, 0, 0). Therefore, the correspondence between the basis vectors is $(A_x',G_y',C_z') \rightarrow (A_x,G_y,C_z)$; $(F_x',C_y',G_z') \rightarrow (G_x,A_y,F_z)$; $(C_x',F_y',A_z') \rightarrow (F_x,C_y,G_z)$; $(G_x',A_y',F_z') \rightarrow (C_x,F_y,A_z)$.

singlet.[13] This means that the occupied orbitals in the (010) planes for the lighter compounds are different with respect to those in the heavier ones. It would mean that the anisotropic terms of the exchange interaction are different in both cases, which would yield to an orientation of the magnetic moments along different directions.

In the specific heat curve, besides the anomaly observed at the temperature for which the magnetic ordering appears, T_N, another anomaly is observed at around $T_{OO} \approx 190$ that is associated with the stabilization of an in-phase orbital ordering. The appearance of an orbital ordering is usually inferred from the presence of a Jahn−Teller ordered state. At room temperature, the difference between the two shortest V−O distances in the VO_6 octahedra is around 0.002 Å, whereas the difference between the shortest and longest distances is around 0.03 Å. Let us point out that this is a small distortion in comparison with the Jahn−Teller effect observed in an e_g^1 orbitally ordered system such as $LaMnO_3$ (≈0.27 Å).[28] In $LuVO_3$, the difference between the shortest V−O distances starts to increase below 190 K, which implies a greater distortion of the VO_6 octahedra. The increase of the Jahn−Teller distortion denotes the establishment of the t_{2g} orbitals ordering.

Conclusions

The magnetization and specific heat measurements have confirmed that $LuVO_3$ undergoes an antiferromagnetic ordering below $T_N \approx 107$ K. The susceptibility measurements give evidence for the presence of a weak ferromagnetism effect. According to the NPD data, below T_N $LuVO_3$ presents a magnetic structure characterized by the propagation vector $k = 0$, with a spin arrangement for the V atoms given by the basis vectors $(0,A_y,F_z)$. The magnetic structure remains stable down to 2 K and the ferromagnetic component is very weak, in good agreement with the susceptibility measurements. The refined ordered magnetic moment at $T =$ 2.4 K for the V atoms is $1.33(6)\mu_B$. There is a dramatic reorganization of the unit-cell parameters a few degrees below T_N, between 94 and 82 K, concomitant with a crystallographic transition from orthorhombic ($Pnma$) to monoclinic ($P2_1/n$). The in-phase arrangement of the V−O chemical bonds in successive *ab* planes suggests an in-phase orbital ordering of the t_{2g} orbitals, compatible with the observed A-type magnetic structure. An additional anomaly at $T_{OO} \approx 190$ K, observed in the thermal evolution of the unit-cell parameters and V−O distances as well as in the specific heat curve is associated with the stabilization of the mentioned in-phase orbital ordering.

Acknowledgment. We thank the CICyT for financial support of the projects MAT2001-0539 and MAT-2002-1329, and we are grateful to ILL for making all facilities available.

CM035314A

(28) Rodríguez-Carvajal, J.; Hennion, M.; Moussa, F.; Moudden, A. H.; Pinsard, L.; Revcolevschi, A. *Phys. Rev. B* **1998**, *57*, R3189.